Journal of the Mechanics and Physics of Solids 61 (2013) 352–369

Contents lists available at SciVerse ScienceDirect

Journal of the Mechanics and Physics of Solids

journal homepage: www.elsevier.com/locate/jmps

A DEM model for soft and hard rocks: Role of grain interlocking on strength

Luc Scholtès [a], Frédéric-Victor Donzé [b,*]

[a] Université de Lorraine/CNRS/CREGU, GéoRessources Laboratory, BP 40, 54501 Vandoeuvre-lès-Nancy, France
[b] Université Joseph Fourier—Grenoble 1/Grenoble INP/CNRS, 3SR Laboratory, Grenoble, France

ARTICLE INFO

Article history:
Received 22 November 2011
Received in revised form
9 October 2012
Accepted 11 October 2012
Available online 23 October 2012

Keywords:
Grain interlocking
Intact rock failure
Brittle behavior
UCS/TS ratio
Brittle ductile transition
Discrete Element Method

ABSTRACT

The Discrete Element Method (DEM) is increasingly used to simulate the behavior of rock. Despite their intrinsic capability to model fracture initiation and propagation starting from simple interaction laws, classical DEM formulations using spherical discrete elements suffer from an intrinsic limitation to properly simulate brittle rock behavior characterized by high values of UCS/TS ratio associated with non-linear failure envelopes, as observed for hard rock like granite. The present paper shows that the increase of the interaction range between the spherical discrete elements, which increases locally the density of interaction forces (or interparticle bonds), can overcome this limitation. It is argued that this solution represents a way to implicitly take into account the degree of interlocking associated to the microstructural complexity of rock. It is thus shown that increasing the degree of interlocking between the discrete elements which represent the rock medium, in addition to enhancing the UCS/TS ratio, results in a non-linear failure envelop characteristic of low porous rocks. This approach improves significantly the potential and predictive capabilities of the DEM for rock modeling purpose. A special emphasis is put on the model ability to capture the fundamental characteristics of brittle rocks in terms of fracture initiation and propagation. The model can reproduce an essential component of brittle rock failure, that is, cohesion weakening and frictional strengthening as a function of rock damage or plastic strain. Based on model predictions, it is finally discussed that frictional strengthening may be at the origin of the brittle ductile transition occurring at high confining pressures.

1. Introduction

The ratio between the uniaxial compressive strength (UCS) and the tensile strength (TS) of brittle rocks, i.e. σ_c/σ_t, constitutes one of their most fundamental characteristics (Altindag and Guney, 2010). Although the compressive strength is the most widely used parameter to characterize rock in the engineering practice (Brady and Brown, 2004), it is now well assumed that brittle failure in rock is mainly governed by tensile rupture mechanisms. A comprehensive model for rock should therefore be able to properly match both its specific compressive and tensile strengths.

The Discrete Element Method (DEM) using spherical discrete elements, which has brought interesting insights to the characterization of failure mechanisms in cohesive frictional materials, is now often used for rock modeling purpose. Due to their discontinuous nature, discrete models can deal with the initiation and propagation of microcracks inside

* Corresponding author.
E-mail address: frederic.donze@3sr-grenoble.fr (F.-V. Donzé).

0022-5096/$ - see front matter © 2012 Elsevier Ltd. All rights reserved.
http://dx.doi.org/10.1016/j.jmps.2012.10.005

heterogeneous media and constitute therefore a powerful tool to study how the microstructure affects the macroscopic properties of geomaterials. However, it seems that there is an intrinsic limitation in the basic formulation of these models: whatever the predefined values of the micromechanical parameters, they are unable to reach high σ_c/σ_t values representative of brittle rocks (Potyondy and Cundall, 2004; Schöpfer et al., 2009), restricting therefore their predictive capabilities to weak or poorly cemented rocks. One consequence is, for example, that calibrating those classical DEM to the compressive strength of a brittle rock results in an over prediction of its tensile strength, which can then be problematic when simulating problems where the stress path may be either tension or compression.

In low-porosity hard rocks like granite or basalt, grain interlocking contributes to high values of the σ_c/σ_t ratio as well as to high internal friction angle. Hence, to overcome the limitation of classical discrete models, it might be necessary to use an additional texture property like irregular shaped discrete elements as proposed by Potyondy and Cundall (2004) or Cho et al. (2007) to improve grain interlocking in order to simulate representative macroscopic behaviors. Indeed, the mechanical behavior of rocks is controlled by their microstructure and results from a combination of mechanisms occurring at the grain scale (Tapponier and Brace, 1976). Thus, a model capable of accurately replicating the microstructure of rock should then permit to properly simulate its macroscopic behavior as it has been demonstrated in 2D by Lan et al. (2010) or Kazerani and Zhao (2010) using polygonal particles. However, although in accordance with the true microstructure of rock, the treatment of non-spherical particles in 3D codes still highly penalizes calculation efficiency, and therefore limits their application to small scale problems.

As an alternative solution, it is possible to implicitly enhance the microstructure of a granular packing by increasing the density of bonds between the constitutive particles. DEM formulations using this feature have already been proposed by Donzé et al. (1997), Fakhimi (2004) or Shiu et al. (2008) for example, but no precise analyses were performed at that time concerning the potential contribution of the method on the macroscopic response of the simulated medium.

The objective of the present paper is to present a 3D DEM formulation capable of properly simulating brittle rock behavior, starting from microstructural considerations. The basic idea is to keep a simple formulation for the DEM in order to ensure high calculation efficiency (i.e. spherical particles and linear elastic contact laws), and then to show how, by simply controlling the degree of interlocking between the constitutive elements, the macroscopic response of the simulated medium can be adjusted to the targeted behavior.

After a brief description of the model features, a sensitivity analysis will be provided in order to emphasize the effects of grain interlocking on the material response. It will then be shown that the proposed approach, besides its predictive capabilities at the macroscopic scale, provides also good agreement in the description of brittle failure processes of rock in terms of crack initiation and propagation.

2. Model presentation

The role of grain interlocking on the macroscopic behavior of granular cohesive materials outlined in this paper was investigated using the YADE Open DEM platform (Kozicki and Donzé, 2008, 2009; Šmilauer et al., 2010), which operates according to a classic DEM algorithm involving two steps. First, based on constitutive laws, interaction forces between Discrete Elements (DE, also referred to as "particles") are computed. Second, Newton's second law is applied to determine, for each DE, the resulting acceleration, which is then time integrated to find its new position. This process is repeated until the simulation is finished.

2.1. Constitutive law

For small deformations a linear elastic response is provided by the use of linear elastic interaction forces between the DE. The interaction force F which represents the action of DE a on DE b can be decomposed into a normal force F_n and a shear force F_s respectively related to the relative normal and incremental shear displacements through the stiffnesses k_n and k_s defined at contact.

The normal interaction force is calculated through the local constitutive law presented in Fig. 1 and can be split into two parts, the compressive and the tensile components.

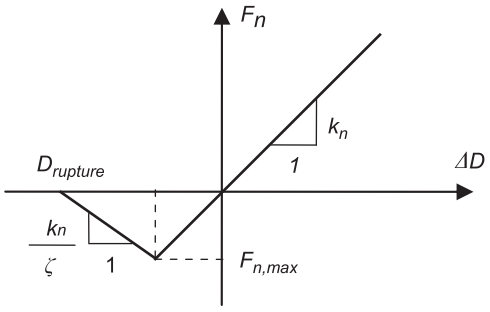

Fig. 1. Normal interaction force between DE.

In compression, F_n is linear and it is given by,

$$F_n = k_n \Delta D \tag{1}$$

where ΔD is the relative displacement between the interacting DE, and k_n is the normal stiffness defined by

$$k_n = E_{eq} \frac{R_a R_b}{(R_a + R_b)} \tag{2}$$

with E_{eq} an equivalent bulk modulus and R_a and R_b the respective radii of the DE.

In tension, the normal interaction force is also linear computed with the same stiffness as in compression for small deformations. The maximum acceptable tensile force $F_{n,max}$ is defined as a function of the tensile strength t such that,

$$F_{n,\max} = -tA_{\text{int}} \tag{3}$$

where $A_{\text{int}} = \pi(_{\min}(R_a,R_b))^2$ is the interacting surface between a and b.

After the maximum tensile force is reached, the stiffness may be modified by a softening factor ζ to control the energy released due to link breakage:

$$F_n = (\Delta D - D_{rupture}) \frac{k_n}{\zeta} \tag{4}$$

When $\Delta D > D_{rupture}$, tensile rupture occurs and the interaction forces are set to zero.

The shear force F_s is computed in an incremental manner by updating its orientation and intensity depending on the increment of shear force $\Delta F_s = k_s \Delta u_s$ which develops at the interaction point, as defined by Hart et al. (1988):

$$F_s = \{F_s\}_{updated} + k_s \Delta u_s \tag{5}$$

with k_s the shear stiffness, which is proportional to k_n and Δu_s the relative incremental tangential displacement.

To model the nonlinear behavior of geomaterials, a modified Mohr-Coulomb model is used (Fig. 2). The maximum admissible shear force $F_{s,max}$ is characterized by the normal force F_n, the cohesion c, the local frictional angle φ_b and the local residual frictional angle φ_c. The maximum shear force is calculated for a bonded interaction according to

$$F_{s,\max} = F_n \tan \varphi_b + cA_{\text{int}} \tag{6}$$

Shear rupture occurs when $F_s \geq F_{s,max}$, the interaction becoming then purely frictional between the initially bonded DE. In the same manner, if new contacts are detected during the simulation, they are treated as purely frictional, with a maximum shear force $F_{s,max}$ defined by,

$$F_{s,\max} = F_n \tan \varphi_c \tag{7}$$

One has to note that both the elastic and the plastic parameters depend on the size of the DE (Eqs.(1)–(7)). This dependency ensures the model's predictions to be independent from its resolution as long as the size of the DE is small enough compared to the size of the considered volume (see Scholtès et al. (2011) or Harthong et al. (2012) for more details). In addition, as the proposed DEM is a fully dynamic formulation, a local non-viscous type damping is used in the model to dissipate kinetic energy (see Potyondy and Cundall (2004) for details). All models described in this paper were run with a damping coefficient of 0.4.

2.2. Interaction range

Unlike the classic granular description of the medium where only discrete elements in contact are connected, e.g. formulation of PFC (Itasca Consulting Group, 2012), ESyS-Particle (Wang and Mora, 2008) or even the first version of YADE (Kozicki and Donzé, 2008, 2009), the proposed approach considers the definition of an interaction range coefficient γ_{int} which can be used to link elements not directly in contact one with another but still in the neighboring zone (Fig. 3). This specific feature provides the possibility to adjust the degree of interlocking of the constitutive particles forming the numerical medium according to the relative microstructural complexity of the material to model.

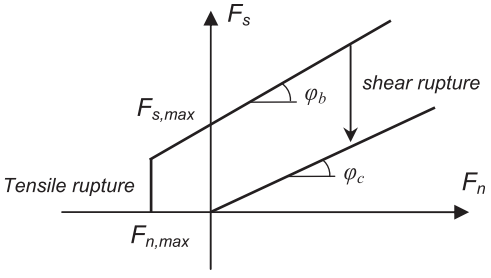

Fig. 2. Rupture criterion used in the model.

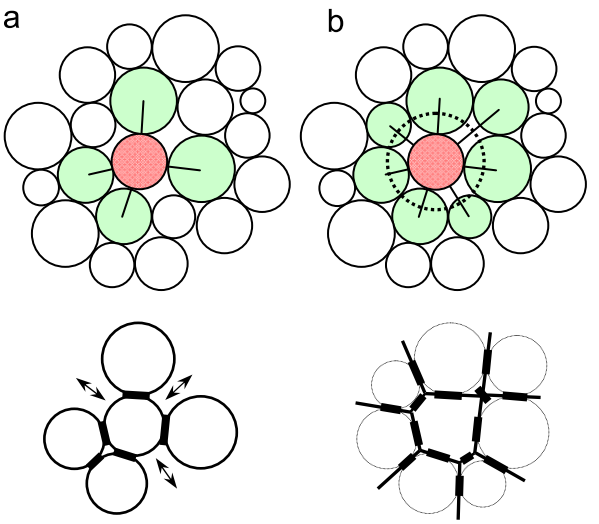

Fig. 3. Illustration of the effect of the interaction range on the contact fabric and grain interlocking: (a) $\gamma_{int}=1$ and (b) $\gamma_{in}>1$.

Given the interaction range coefficient γ_{int}, bonds are created between DE of radius R_i if their respective interacting ranges defined by $\gamma_{int}R_i$ overlap before the first time step of the simulation (Donzé et al., 1997). The number of bonds per particle (also referred to as the coordination number N in the following), can therefore be predefined regardless of the specific texture of the considered packing. Nevertheless, care should be taken to avoid particles embedded in between interacting pairs by checking that the interaction range is not greater than the one defined by the relative distribution of particle diameters inside the medium (e.g. if $R_{max}/R_{min}=2$, γ_{int} must not be larger than 1.5). In a same manner, the initial packing density must be maximal in order to minimize the effect of collapsing pores inside the medium when a bond fails between non-contacting DE.

In order to avoid any lock in stresses in the numerical assembly, interaction forces are computed according to Eq. (1) by updating the relative displacement ΔD between DE as

$$\Delta D = D - D_{eq} \tag{8}$$

With D the distance between the centers of the DE and D_{eq} the equilibrium distance defined as

$$D_{eq} = \gamma_{\text{int}}(R_a + R_b) \tag{9}$$

One has to note that the interaction range is set to its default value ($\gamma_{\text{int}}=1$) after the initial detection time step, letting new contacts occur between strictly contacting DE, as in classical DEM simulations of granular media.

The present method shares some similarity with the clump logic proposed by Cho et al. (2007) without the associated computational difficulties. Indeed, the resulting medium consists in a packing where particles are not anymore described by spheres interacting through unique contact planes one with another, rather than by complex shaped equivalent particles sharing multiple contact planes all together (see Fig. 3). Doing so, particle interlocking is therefore increased and should play a significant role on the internal friction as well as on the strength properties of the simulated medium without complicating the constitutive equations. Since the elastic parameters and the tensile rupture depend on the size of the DE, the adjustment of the interaction range γ_{int} to keep N constant whatever the considered packing ensures that the model's results are independent from its resolution (Scholtès et al., 2011).

3. Influence of the degree of interlocking on the macroscopic behavior

The purpose of this paper being to investigate the role of grain interlocking on the macroscopic behavior of granular cohesive materials, models predictions were examined by performing uniaxial tension and compressive test simulations on a numerical assembly made up of 10,000 DE with a uniform particle size distribution such as $R_{max}/R_{min}=2$ (Fig. 4). A preliminary study showed that 10,000 DE provides the best compromise regarding both computational efficiency and representativeness in terms of behavior predictions since it constitutes the inferior limit above which the simulated macroscopic behavior is independent on the model resolution. One can note that 10,000 DE specimens contain about 20 particles across its smallest dimension which corresponds to the limit recommended by the International Society for Rock Mechanics (ISRM) concerning the minimum dimension of the specimen in regards to its largest mineral grain size.

Direct tensile test were chosen to characterize the tensile strength of the specimen as the numerical implementation is relatively straightforward and does not suffer from the numerous difficulties encountered experimentally (Coviello et al., 2005). Particles forming the axially opposite boundaries of the specimen are identified and assigned to a constant velocity. In order to avoid any stress concentration at the boundaries, a recovery zone was defined where interparticle bonds cannot break (Fig. 4(a)). Doing so, the complete failure of the sample was then able to occur far away from the boundaries as illustrated in Fig. 6, ensuring

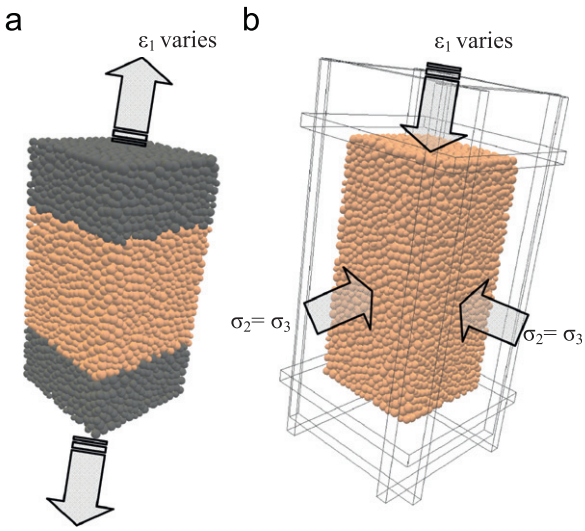

Fig. 4. Numerical assembly used in this study, (a) direct tension test configuration and (b) compression test configuration. Dark areas indicate zone of unbreakable bonds.

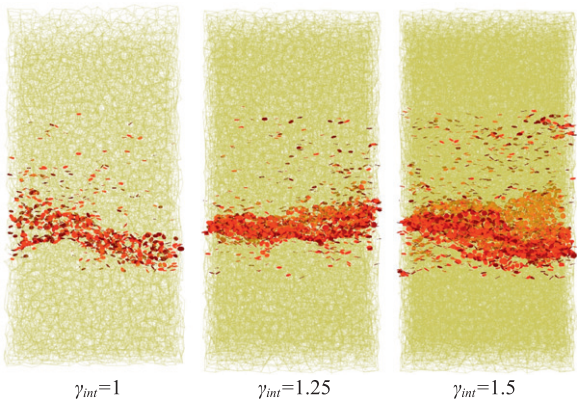

Fig. 5. Crack (darker discs) distribution resulting from direct tension test simulations performed on the same assembly for different values of the interaction range γ_{int} (see Table 2 for microparameters).

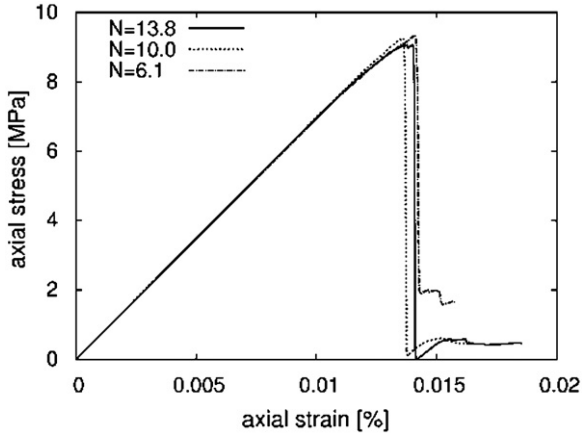

Fig. 6. Stress–strain curves obtained from direct tension test simulations performed on the same assembly with different coordination numbers *N* but with the same macroscopic behavior (see Table 2 for microparameters).

the intrinsic nature of the measured tensile strength. Compressive test simulations were performed through the use of rigid platens moving simultaneously one toward the other, the confinement being controlled through lateral walls (Fig. 4(b)). For every test simulations, the loading rate was set slow enough to ensure that the quasi static conditions were met without any artifacts induced by the damping coefficient value. Quasi static conditions can be confirmed for example by demonstrating that reducing the loading rate does not alter the measured macroscopic strength.

3.1. Direct tension tests

Because it was extensively studied in the laboratory, Lac du Bonnet granite is often cited as a reference when it comes to the modeling of brittle rocks. Moreover, as numerous attempts were made to simulate its behavior using DEM (Potyondy and Cundall, 2004; Fakhimi 2004; Cho et al. 2007; Wang and Tonon 2009), Lac du Bonnet granite was therefore chosen here to assess the capabilities of the proposed model in regards to what already exists in the literature. Its mechanical properties are presented in Table 1.

Unlike in previous attempts designated to simulate Lac du Bonnet granite behavior, the calibration of the present numerical model was chosen to be made starting from direct tensile tests simulations, assuming that the tensile strength is the critical mechanical parameter. A series of direct tensile tests was then performed on the same numerical assembly for different values of the interaction range ($\gamma_{int}=\{1;\ 1.25;\ 1.5\}$), corresponding to different values of the coordination number N (see Table 2). As presented in Fig. 6, it was possible to match the same macroscopic tensile behavior for each value of γ_{int} either in terms of Young's modulus or tensile strength, by simply adjusting the interparticle stiffness E_{eq} and tensile strength t.

Due to the nature of the loading, the values of φ and c/t do not have any influence on the tensile strength of the model, assuming their calibration has to be done through adapted loading paths like compressive tests simulations performed at different confining pressures as presented in the following sections.

Looking at the crack distribution inside the assembly at failure (Fig. 5), one can already see a difference in the simulated responses in terms of the micromechanical phenomena. Indeed, the number of interparticle bonds (N) in the medium increases with the value of the interaction range γ_{int}. The local tensile strength of the bonds needs therefore to be smaller for high values of N in order to produce an equivalent macroscopic tensile strength (see Table 2). The number of microcracks at failure thus tends to be larger for high values of N with a more diffuse distribution around the final failure surface. One could see here similarities with the extension of the fracture process zone (FPZ) which has been observed to be greater in low porosity hard rocks than in porous soft ones (Stanchits and Dresen, 2003).

3.2. Uniaxial compression tests

The most common method to characterize mechanical properties of rocks consists in performing uniaxial compression tests. However, in real experiments, compressive strength can be markedly affected by the presence of pre-existing microcracks and end-boundary conditions as noted for example by Peng and Johnson (1972) from laboratory tests on Chelmsford granite. One of the most affecting causes of discrepancy is linked to the condition of friction at the interface between the specimen and the loading platens. For instance, high frictional constraint at the interface tends to favor the resistance of the specimen. The latter becomes slightly barrel shaped during loading and generally fails either by the formation of a cone at each end or by flaking of pieces at mid-height. On the contrary, perfect lubrication tends to penalize the resistance of the specimen, with early appearance of cracks near the ends of the specimen leading to longitudinal splitting.

In order to investigate the boundary effects on model predictions, a series of uniaxial compressive tests were performed for different friction conditions between the particles forming the numerical specimen and the loading platens (Fig. 7).

Table 1
Material properties of Lac du Bonnet granite after Potyondy and Cundall (2004) and after Martin (1997).

Density (kg/m^3)	E (GPa)	v	σ_c (MPa)	σ_t (MPa)
2640	69	0.26	200	9.3

Table 2
Model micro-parameters used to simulate Lac du Bonnet Granite behavior in tension for different interaction ranges γ_{int}.

γ_{int}	N	E_{eq} (GPa)	k_n/k_s	t (MPa)	c (MPa)	φ (°)
1	6.1	230	2.5	22	10t	25
1.25	10.0	112	2.5	11.5	10t	25
1.5	13.8	68	2.5	7	10t	25

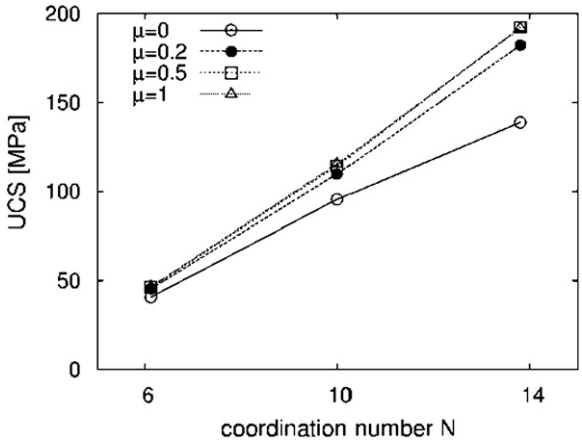

Fig. 7. Effect of friction at the interface (μ) between the loading platens and the specimen on the uniaxial compressive strength for different values of the coordination number N but same macroscopic tensile behavior (parameters defined in Table 2).

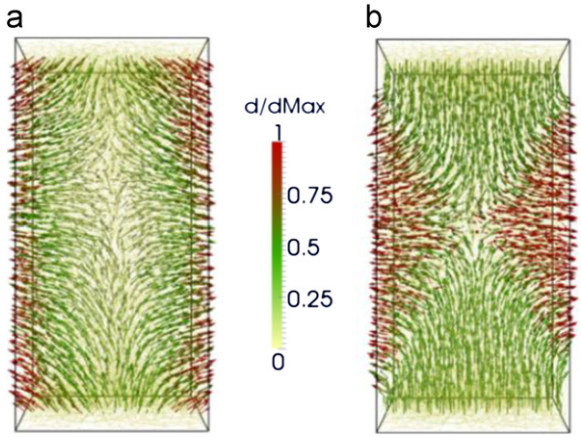

Fig. 8. Effect of the boundary conditions on the failure mode of the numerical model. Cross-sectional deformation field at failure: (a) frictionless loading platens and (b) frictional loading platens.

As shown in Fig. 7, frictional constraint at the interface, even for low values of the coefficient of friction μ, definitely tends to favor the resistance of the specimen with higher UCS whatever the considered density of interparticle bonds. Interestingly, the discrepancy tends to increase with the compressive strength of the specimen.

In terms of fracturing and deformation patterns, model predictions seem also to confirm Peng's results with a fairly uniform deformation field induced to the specimen associated to longitudinal splitting when frictionless platens are used and appearance of cone like shapes and associated buckling when friction is introduced at the interface (Fig. 8).

Because experimental uniaxial compression tests generally tend to produce results in accordance with the simulations performed with a frictional constraint (barrel shape, either cone formation or faulting from the corners) due to the extreme difficulty to avoid friction in experiments, the choice was made to use frictional platens for the study imposing $\mu=0.5$ as a first approximation. However, one has to keep in mind that the resulting strengths belong to the higher range and do not correspond to ideal homogeneous loading conditions.

The stress–strain curves obtained from uniaxial compression tests performed on numerical specimens calibrated to Lac du Bonnet Granite tensile strength (see Fig. 6), for different interparticle bond densities are compared in Fig. 9.

It can be seen that when the number of bonds per particle increases, the brittleness (or σ_c/σ_t ratio) increases. However, because these results were obtained for a given set of microparameters, the following sections presents a systematic investigation about the effect of the microproperties on the ratio of tensile to compressive strengths.

3.3. *Effect of microparameters on the strength ratio*

The study focuses here on the microparameters likely to influence the macroscopic strength of the model. For consistency, care was taken, however, to keep the elastic behavior and tensile strength of the model in accordance with

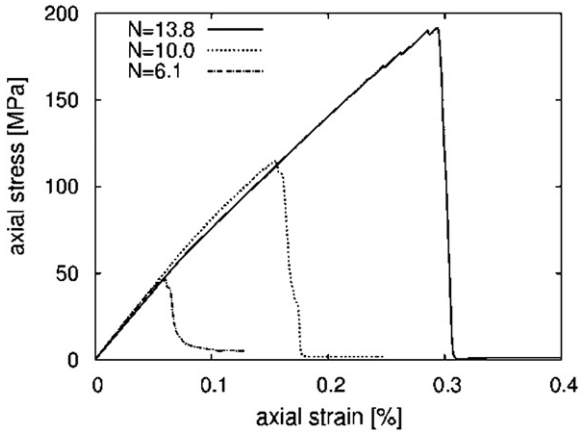

Fig. 9. Stress–strain curves obtained from uniaxial compressive test simulations performed on the same assembly for different values of the coordination number N but same macroscopic tensile behavior (see Table 2 for microparameters).

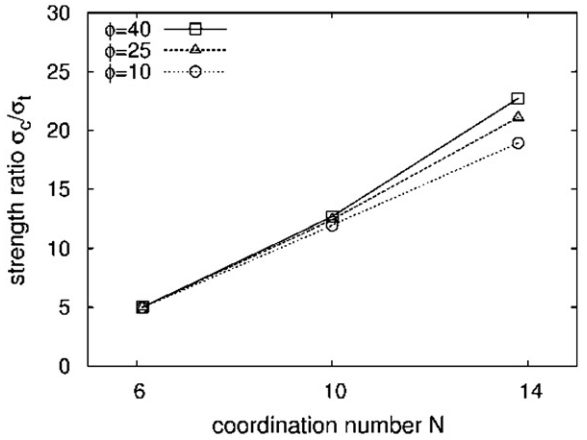

Fig. 10. Effect of the coefficient of friction on the ratio of tensile strength to compressive strength for different bond densities but same bond strength ratio $c/t=10$.

those of Lac du Bonnet granite. It can be seen that keeping constant all the parameters controlling the elastic response, i.e. E_{eq}, k_n/k_s, as well as the local tensile strength t produced identical responses to the ones presented in Fig. 7.

In the present model, bonds can break either by tensile or shear rupture mode, with a loading capacity which depends on both the maximum admissible normal and shear forces $F_{n,\max}$ and $F_{s,\max}$ respectively (see Section 2). While $F_{n,max}$ is kept constant to ensure a constant tensile strength, we focus here on the influence of the parameters controlling $F_{s,max}$. As defined in Eq. (6), $F_{s,max}$ depends on the normal force through the Coulomb criterion. One has therefore to assess the respective effect of the cohesion c and of the interparticle friction φ on the macroscopic strength.

The effect of interparticle friction on the σ_c/σ_t ratio for different values of the coordination number N is shown in Fig. 10. In accordance with the results of Cho et al. (2007), it seems that, whatever the density of bonds, increasing the coefficient of friction at contact does not have a significant effect on the σ_c/σ_t ratio. One can see, however, that models with higher values of N present higher macroscopic strength ratios.

As for any other DEM, the characteristic parameter that controls the macroscopic strength is the ratio between the normal and shear bond strengths c/t at contact. For instance, increasing the c/t ratio tends to favor brittle failure as interparticle bonds then preferentially break through local tensile microcracking rather than through shear rupture. However, as depicted in Fig. 11, it seems that increasing c/t has very little influence on the σ_c/σ_t ratio if it is not associated with an increase of the number of bonds in the medium. For instance, when bonds are strictly present at contacts ($\gamma_{int}=1$, $N=6.1$), the σ_c/σ_t ratio reaches 5, which is in agreement with classic spherical DEM formulations (Cho et al., 2007; Potyondy and Cundall, 2004). On the contrary, σ_c/σ_t can reach values greater than 20 for high densities of interparticle bonds; confirming Potyondy and Cundall (2004) findings that only a modification of the microstructure can readily improve the predictive capabilities of the DEM for rock modeling purposes.

One has to note that, even without any introduction of explicit rolling resistance between the DE as proposed in Iwashita and Oda (1998), Plassiard et al. (2009) and Wang and Mora (2008) for examples, increasing the number of

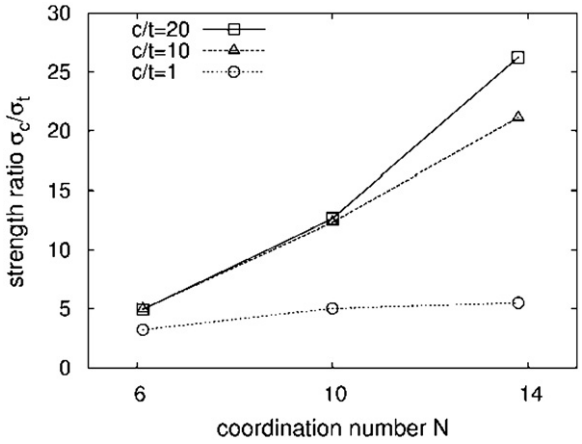

Fig. 11. Effect of bond strength ratio *c/t* on the ratio of tensile strength to compressive strength for different bond densities but same interparticle friction angle $\varphi=25^\circ$.

interparticle bonds, which increases the degree of interlocking between the DE, produces two effects on the compressive strength. First, by restricting particles rotations, it implicitly enhances moment loading within the medium. Secondly, because the number of contact planes between the DE is increased, the internal friction is increased as well. This is the combination of those two effects which is most probably at the origin of the strength increase as noted previously by Cho et al. (2007).

From the results discussed above, it appears that controlling the density of bonds in discrete models allows for simulating high σ_c/σ_t ratios in accordance with what is usually observed for brittle rock. Moreover, contrary to the use of clump logic or any other complex geometrical description of the constitutive particles which computational need would be prohibitive in 3D ((Cho et al., 2007; Lan et al., 2010; Kazerani and Zhao, 2010), presented results only in 2D), the efficiency of the method is therefore not modified and can be applied to relatively large scale 3D simulations as proposed in (Scholtès and Donzé, 2012). The other interesting result is that, by increasing the density of bonds inside the medium, macro-failure is associated to a relatively larger number of microcracks which seems to be in accordance with experimental observations made concerning failure in brittle rocks (Stanchits and Dresen, 2003).

3.4. Triaxial testing: effect of the confining pressure

The results from the previous section show that increasing the degree of interlocking between the constitutive particles of a granular medium influences the brittleness of the material response. In order to assess the effect of the confining pressure, a series of triaxial tests was performed on the same numerical specimens, for different values of the coordination number *N*. As shown in Fig. 4, the loading is applied through rigid frictionless boundary walls as in true triaxial cells. As suggested by several authors (Potyondy and Cundall, 2004; Wang and Tonon, 2009), such boundaries tend to inhibit specimen bulging as boundary particles are aligned with the surrounding walls. The drawback is that, on one hand, the failure process and deformation are constrained by the boundaries and may therefore differ from the experiments, but on the other hand, the applied loading is more homogeneously distributed.

The failure envelopes obtained on the numerical specimen for the range of coordination numbers *N* previously defined (Table 2) are presented in Fig. 12. As a reference, the Hoek–Brown failure criterion (HB) fitted to the experimental results obtained by Martin and Chandler (1994) on Lac du Bonnet Granite is plotted as well. The HB criterion, which is used for its capability to match the specific non-linear failure envelope of rock, is defined as follows:

$$\sigma_1=\sigma_3+\sigma_c\left(m\frac{\sigma_3}{\sigma_c}+s\right)^{0.5} \tag{10}$$

where σ_c is the Unconfined Compressive Strength (UCS) and m and s are material constants. For Lac du Bonnet granite, $\sigma_c=224$ MPa, $m=28$ and $s=1$ (Martin and Chandler, 1994).

A key feature emerges from the numerical results in the compressive region. For instance, contrary to the linear failure envelope obtained using the classic DEM spherical approach ($\gamma_{int}=1$, $N=6.1$), the strengths resulting from the models with high degrees of interlocking ($\gamma_{int}>1$) provide non-linear failure envelopes in accordance with what is generally observed for rock, supporting therefore the pertinence of the model. One can also note that the values of the UCS generally tend to be in accordance with the shape of the HB criterion even though obtained from non-uniform loading conditions (see Section 3.2). This latter remark would need further study. Nevertheless, it raises the question concerning the influence of the loading conditions on the characterization of material strength and confirms the necessity to carry the calibration of numerical models using multiple stress paths rather than just one of them (as it is often done by only using the UCS value).

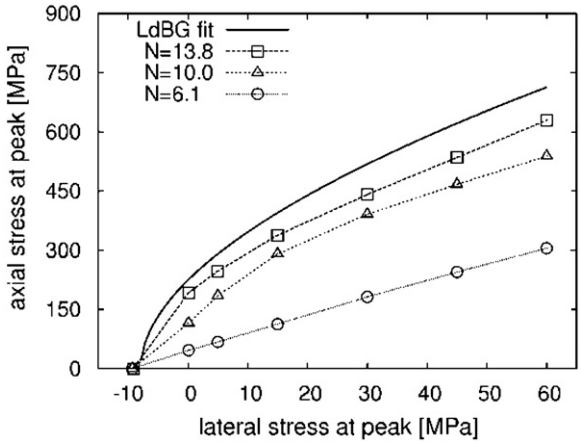

Fig. 12. Failure envelopes obtained from triaxial compression tests performed on the same numerical sample for different bond densities (parameters defined in Table 2). Hoek–Brown criterion fitted to experimental results obtained on Lac du Bonnet Granite (LdBG) is given for illustration purpose.

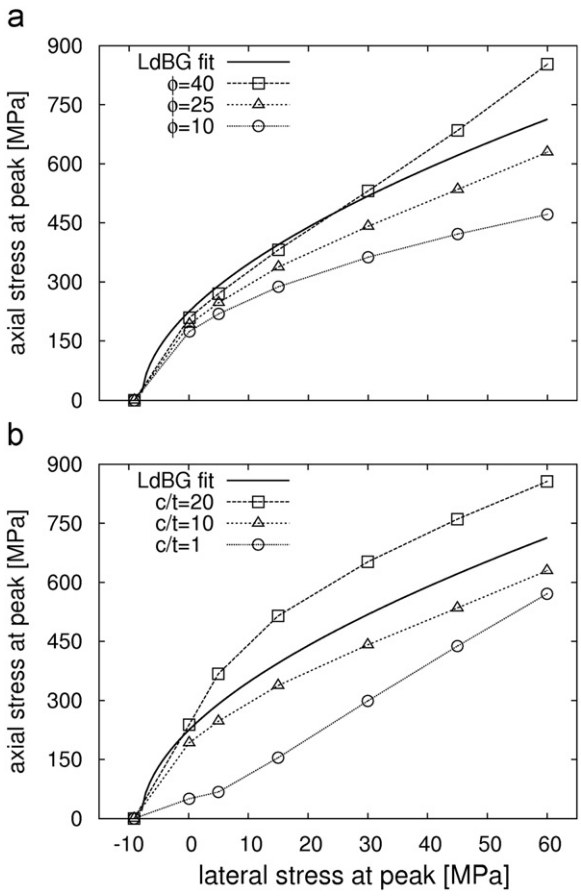

Fig. 13. Effect of the model microparameters on the shape of the failure envelope: results obtained from triaxial compression tests performed on the same numerical sample ($N=13.8$) for different values of the interparticle friction angle φ (a) and of the tensile to shear bond strength ratio c/t (b). Hoek–Brown criterion fitted to experimental results obtained on Lac du Bonnet Granite (LdBG) is given for illustration purpose.

In order to investigate the effect of the microparameters on the shape of the rupture envelope, another series of triaxial tests was run for different values of the c/t ratio and of the interparticle friction angle φ. For this analysis, the model with the highest coordination number ($N=13.8$) was chosen as its response is the closest to the one of Lac du Bonnet granite (Fig. 13).

Contrary to classic spherical DEM formulations for which adjusting contact parameters have just little effect on the material response, it is shown here that, with the enhancement in the degree of interlocking, contact microproperties do have an original and significant influence on the macroscopic behavior. Respectively, if the interparticle friction angle is strongly related to the internal friction of the medium (slope of the failure envelope), the local value of the cohesion c directly contributes to the macroscopic cohesion (t was kept constant here, making the cohesion dependent on the value of c only). This finding is of primary interest as it will greatly ease the calibration procedure.

In order to support the predictive capabilities of the model, the proposed approach is shown, in the following sections, to be suitable for real rock modeling by comparing its predictions to referenced experimental results.

4. Comparison with real rocks

The choice is made here to reproduce the behavior of two distinct rock types, the Lac du Bonnet granite (after experiments carried out by Martin and Chandler (1994) and Martin (1997)) and the Fontainebleau sandstone (after experiments done by Sulem and Ouffroukh (2006)), representative of hard and soft brittle rocks respectively. According to the previous results, in regards of the respective effects of the model parameters on the material response, the calibration procedure was run as follow:

1. Choice of a coordination number N allowing matching the desired tensile strength to compressive strength ratio σ_c/σ_t. As a first approximation, from the authors' experience the c/t ratio is taken equal to the macroscopic σ_c/σ_t ratio. Looking first arbitrary, this option seems however to capture the micromechanisms usually observed experimentally as tensile cracking is representative of the brittleness of the material.
2. Determination of the elastic parameters E_{eq} and k_n/k_s in order to match the elastic properties (Young modulus and Poisson ratio) by running either tensile or compression tests.
3. Determination of the local tensile strength t in order to match the tensile strength of the material by running tensile tests.
4. Determination of the interparticle friction angle φ in order to match the slope of the failure envelope by running a series of triaxial compression tests at different confining pressures.

The microparameters resulting from the calibration procedure are listed in Table 3 for both granite and sandstone. Models predictions in terms of stress–strain responses and failure envelopes are presented in Figs. 14 and 15. The range of confining pressures was selected to correspond to the one used in the experiments. Comparisons are essentially based on the failure criteria used by the authors to fit their respective experimental results. However, care was taken to ensure that the elastic properties of the models match those of the real materials.

In both cases, the model is able to fairly match the experimental failure envelopes as well as the typical σ_c/σ_t ratios (20 for granite and 10 for sandstone). In addition, the model reproduces the characteristic transition from plastic brittle to plastic ductile behavior with the increase of the confining pressure. In accordance with theory, this transition is associated to a decrease of the dilative capacity of the medium with the confinement as depicted by the decrease of the slope of the volumetric curves in the post-peak regime.

The interesting point here is the respective values of the coordination number N. For instance, N is higher for the model reproducing Lac du Bonnet granite behavior ($N=13$) than for the one that reproduces Fontainebleau sandstone's ($N=10$). Care has to be taken here because of the relative microstructural simplicity of the model compared to the real microstructure of rock but one could argue that the difference in the degree of grain interlocking is in accordance with the respective microstructure of both rock types (Fig. 16).

4.1. Fracturing processes

As a characteristic feature of DEM modeling, the macro-failure of the numerical medium is caused by the occurrence and coalescence of local microcracks in a way similar to the phenomenon involved in real rock. It is therefore important to have an idea about the evolution of contact failures in regards to the macroscopic response of the specimen.

The cumulative microcracking occurring during a triaxial test simulation performed on the model calibrated to Lac du Bonnet granite under a confining pressure of 5 MPa is presented in Fig. 17. As a result of the high bond strength ratio c/t used here, microcracking occurs through local tensile rupture only. In accordance with experimental observations of brittle

Table 3
Microparameters calibrated to model Lac du Bonnet Granite after Martin (1997) and Fontainebleau sandstone after Sulem and Ouffroukh (2006).

Rock type	Density (kg/m^3)	N	E_{eq} (GPa)	k_n/k_s	t (MPa)	c (MPa)	φ (°)
Granite	2640	13	68	2.5	8	1600	10
Sandstone	2600	10	50	3	4.5	45	18

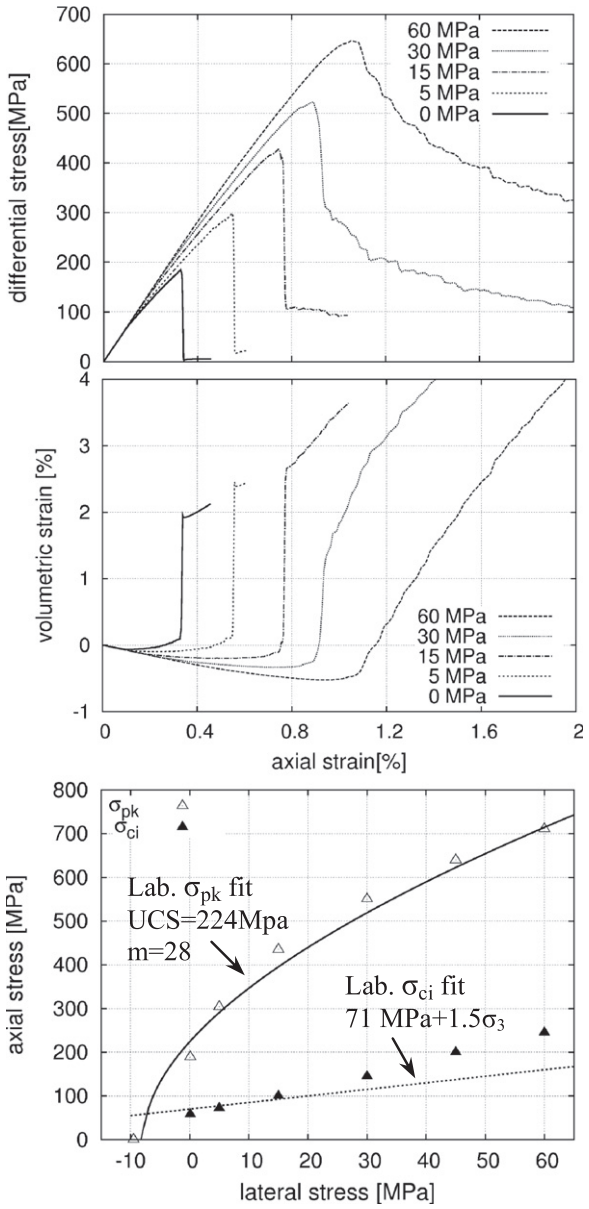

Fig. 14. Results from numerical simulations performed on a model calibrated to Lac du Bonnet granite (see Table 3): stress–strain curves for different confining pressures and comparison of the predicted failure envelope with Hoek–Brown criterion fitted from experiments by Martin (1997). The axial stress at peak is noted σ_{pk}, and σ_{ci} is the axial stress at crack initiation.

failure in rock (Brace et al., 1966; Martin and Chandler, 1994; Eberhardt et al. 1998), microcracking induced by compressive loading can be classified into several distinct phases.

First, one can already note that, contrary to real rock specimens, the model is built as an intact medium and therefore does not contain any pre-existing cracks. Thus, the initial crack closure and associated increase in axial stiffness usually observed during the first stages of the loading does not exist. A solution would consist here in deleting a certain amount of interparticle bonds in the assembly as done by (Schöpfer et al., 2009) to take into account pre-existing cracks, but it has not been tested here and would require further investigations. The specimen behaves therefore elastically at the beginning of the loading with very little damage induced to its microstructure as indicated by the linearity of both stress and strain curves. Very few cracks are generated inside the sample during this stage of the loading (snapshot I presents all the cracks accumulated during the elastic phase).

The end of this first elastic phase corresponds to the onset of dilation as indicated by the typical depart from linearity of the volumetric strain curve. Volume begins to increase relative to elastic changes due to the appearance of axially aligned

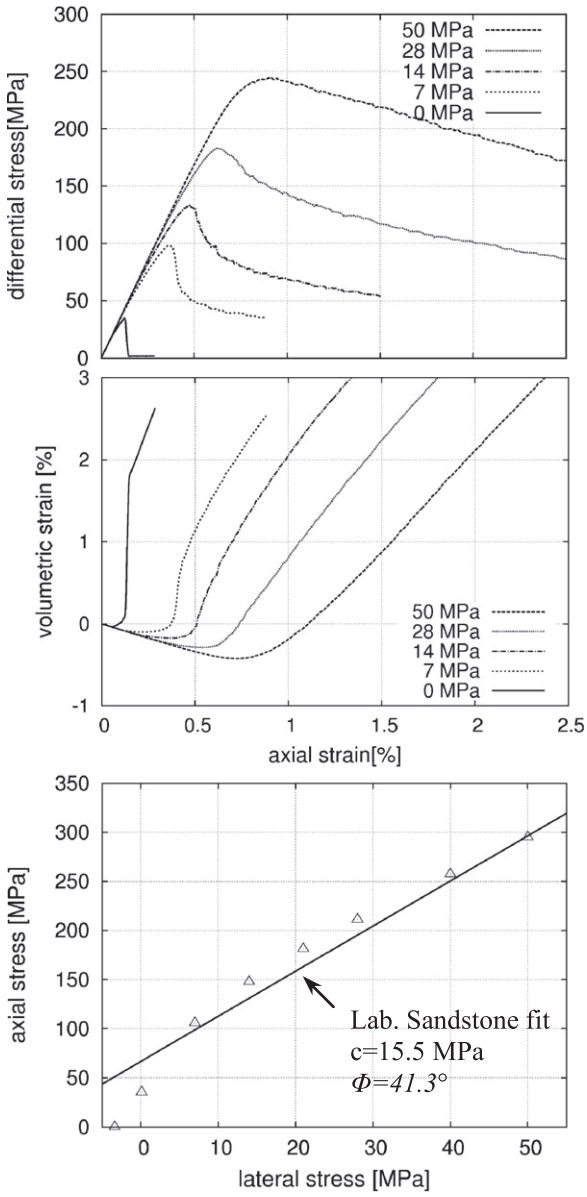

Fig. 15. Results from numerical simulations performed on a model calibrated to Fontainebleau sandstone (see Table 3): stress–strain curves for different confining pressures and comparison of the predicted failure envelope with Mohr-Coulomb criterion fitted from experiments by Sulem and Ouffroukh (2006).

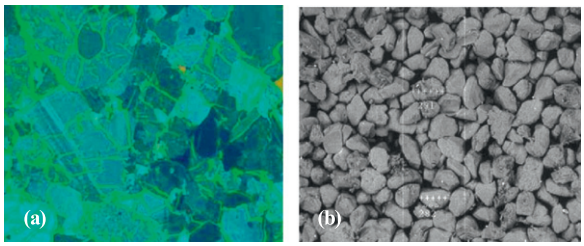

Fig. 16. Microphotographs of (a) Lac du Bonnet granite (after Lan et al. (2010) and (b) Fontainebleau sandstone (after Sulem and Ouffroukh (2006)).

cracks homogeneously distributed inside the medium (about 2% of the number of cracks accumulated at the peak strength). As observed experimentally, this state corresponds to a characteristic stress level, defined as the crack initiation stress σ_{ci} (Martin and Chandler, 1994), which is approximately equal to one third of the final peak strength (σ_{pk}).

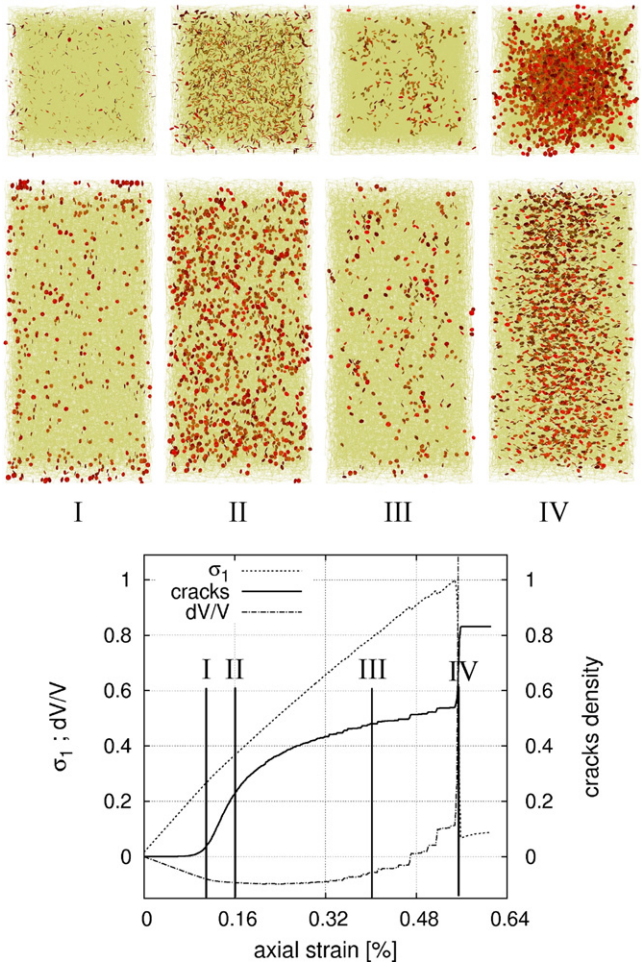

Fig. 17. History of interparticle bond failures and sequential snapshots of the microcrack distribution taken at different intervals during a triaxial compressive test simulation performed on a model calibrated to Lac du Bonnet granite under 5 MPa confinement. The sequential snapshots respectively illustrate characteristic fracturing phases: crack initiation (I); homogeneous crack development (II); crack coalescence associated to dilatancy (III) and macro-failure (IV).

The values of σ_{ci} obtained for all confining pressures can be approximated by the following linear relationship:

$$\sigma_1 = 0.3\sigma_{ucs} + 2.6\sigma_3 \tag{11}$$

Even though slightly different from the experimental observations made for Lac du Bonnet Granite ($\sigma_1 = 70 + 1.5\sigma_3$), Eq. (11) is however in good agreement with the experimental observations generally made on various brittle rock types concerning damage initiation (Brace et al., 1966; Pestman and Van Muntser, 1996.

Following crack initiation, microcracking develops homogeneously inside the medium at a fairly constant rate, progressively damaging the entire specimen as shown in snapshot II (cyclic loading of the specimen in this region would demonstrate a degradation of its elastic properties). Then, the rate of microcracking tends to reduce before stabilizing at a stress level coinciding with the reversal of the volumetric strain curve (axial strain = 0.32%). This stress level, defined as the crack damage stress σ_{cd} by Martin and Chandler (1994) corresponds approximately to two third of the final peak strength, which is, again, in good agreement with the experimental observations made on Lac du Bonnet granite ($\sigma_{cd} = 0.7\ \sigma_{pk}$). From this stage, fracturing occurs as a result of clusters of cracks whose orientation is preferentially inclined compared to the axis of the loading (snapshot III), suggesting the occurrence of crack coalescence.

Finally, the total failure of the specimen occurs, associated to a sudden increase in the rate of microcracking characteristic of the formation of a macro-failure surface across the specimen. Due to the condition of the loading (see Section 3.2), the failure of the sample is associated here with a fairly diffuse axial splitting (snapshot IV) rather than by localized transverse shear banding as often observed experimentally. At this stage, the cohesive strength of the medium is totally destroyed and the residual strength is mobilized through friction as proven by the absence of additional microcracking in the post peak region.

From the previous considerations, it appears that the method provides all the fundamental components for the modeling of brittle failure. In addition to the capability to properly simulate the macroscopic behavior of real brittle geomaterials, failure results from the growth and accumulation of tensile cracks whose evolution can be quantified by normalizing the stresses and strains required to pass from one stage of crack development to another.

4.2. Effect of the confining pressure

As noted earlier, the post peak response of the numerical specimen tends to evolve from plastic brittle to plastic ductile with the increase of the confining pressure, the apparent ductility corresponding to the generation of a residual strength after failure. This phenomenon of frictional strengthening constitutes an essential component of brittle rock behavior as stated previously by several authors (Byerlee, 1968; Martin and Chandler, 1994; Hajiabdolmajid et al., 2002). Indeed, as already observed in soils (Schmertmann and Osterberg, 1960), the cohesional and frictional strength of rocks are not necessarily mobilized simultaneously. For instance, in rock, friction is only mobilized when the cohesional component of strength is significantly reduced as a result of damage and/or plastic strain.

In order to investigate more specifically the characteristic transition from a predominantly cohesional toward a frictional strength controlled mode of failure, a new series of triaxial test simulations were performed on the model calibrated to Lac du Bonnet granite at high confining pressures. As argued by Hajiabdolmajid et al. (2002) in regards to Latjai (1969) experiments on solid plaster blocks, if damage induces the conversion of the cohesive medium into a frictional one, one should therefore expect that the behavior of rock, even brittle, is frictional under high confining pressures. Under those considerations, the yield envelope should therefore be "bi-linear" with a typical non-linear part at low confinement where failure is primarily controlled by tensile fracturing and a linear part at high confinement where failure is mainly controlled through frictional and shear processes. As noted by (Hajiabdolmajid et al., 2002), this notion that the failure envelope is bi-linear for cohesive materials is not new and has already been demonstrated by Schofield and Worth (1966) for stiff over-consolidated clays.

The stress–strain curves as well as the corresponding failure envelope obtained for an extended range of confining pressures are presented in Fig. 18. As described by theory, the predicted failure envelope provides both characteristic parts of respectively cohesional and frictional controlled failure mode. Moreover, in agreement with Latjai's experiments, the transition is effective as soon as the confining pressure exceeds the uniaxial compressive strength of the specimen ($UCS^{model} \approx 190$ MPa).

One can observe on the triaxial curves that the change in the slope of the failure envelope corresponds to the appearance of strain hardening in the "post-peak" regime where dilatancy is not anymore associated to softening as for the tests performed at lower confining pressures, but to an increase of the strength as a function of plastic strain.

Comparing the history of contact failure at 300 MPa (Fig. 19) to the one obtained at 5 MPa (Fig. 17), one can note that the ductility of the behavior is reflected by the absence of a sudden increase in the rate of microcracking when the strength reaches its maximum: the confinement tends to prevent unstable crack growth as well as fracture coalescence. In addition, contrary to the low confinement simulation where failure occurs through longitudinal splitting associated to tensile microcracking (Fig. 20(a)), failure at high confinement appears to be due to the formation of an inclined shear fault going across the specimen (Fig. 20(b)). An analysis on the nature of the microcracks indicates that this shear failure is predominantly associated to local shear rupture of the interparticle bonds. Hence, at peak, the number of shear cracks is approximately two times higher than the number of tensile cracks, proving that tensile fracturing is prevented by the confinement.

In addition to its ability to accurately capture rock behavior in the brittle regime, the model appears also to be able of reproducing fundamental aspects of rock behavior under high confining pressures. In particular, the frictional mobilization of strength as a result of the increase of the confining pressure is captured. However, due to its intrinsic formulation, the model is not able to take into account the occurrence of grain cracking or crushing which can be of significant importance in the mechanisms of real rock failure (Sulem and Ouffroukh, 2006). It was not the purpose of the current study to describe such a phenomenon (see Marketos and Bolton (2009) for example) and care should then be taken concerning model predictions in the upper range of the confining pressures. Nevertheless, the results presented here tends to confirm Byerlee's assumption concerning the brittle ductile transition in rock (Byerlee, 1968) in the sense that ductile behavior is observed as soon as the shear stress required to cause sliding along a fault surface (the frictional strength) is superior or equal to the shear stress required to actually form a fault (the fracture or cohesional strength). With the increase of the confinement, friction increases to such an extent that it requires much stress to overcome friction than it does to cause brittle faulting. Failure is thus associated to strain hardening due to friction strengthening rather than to strain softening as observed in Fig. 18, the transition pressure being approximately equal to the uniaxial compressive strength of the specimen.

The results provided here would obviously need further investigation in terms of micromechanisms; in particular, one could investigate if deformation mechanisms within brittle rock at high confining pressures are equivalent to the types of deformation processes acting within granular materials similar to what have been observed for concrete (Gabet et al., 2008; Tran et al., 2011). Nevertheless, the results discussed here already give additional supports toward the predictive capabilities of the proposed model to reproduce realistic rock behavior in an extensive range of confining pressures.

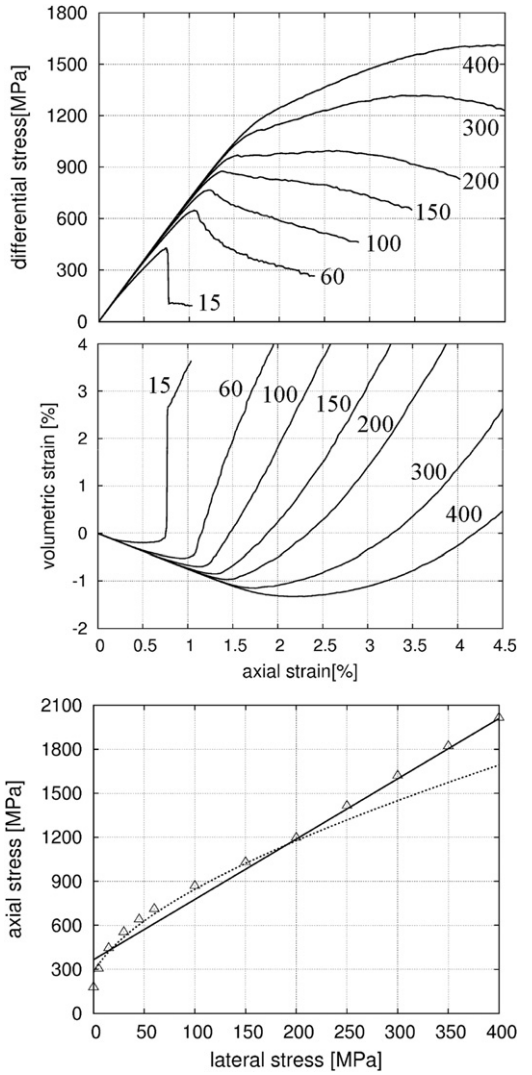

Fig. 18. Results from triaxial test simulations performed at high confining pressures on a model calibrated to the Lac du Bonnet granite showing the bilinear nature of the failure envelope. Numbers at the end of the curves indicate the confining pressures.

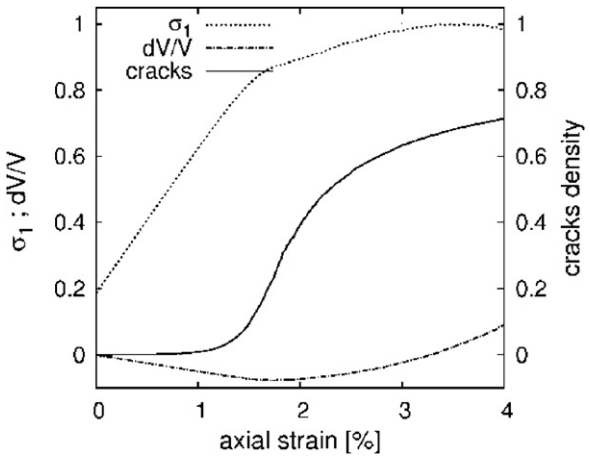

Fig. 19. History of contact failure during a triaxial compressive test simulation performed on a model calibrated to Lac du Bonnet granite under 300 MPa confinement.

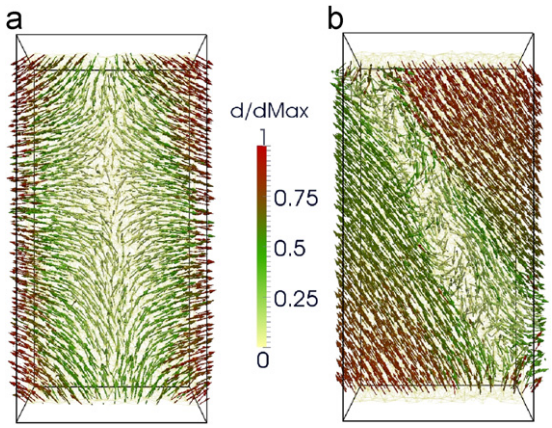

Fig. 20. Effect of the confining pressure on the failure mode of the numerical model: cross-sectional deformation fields at failure for confining pressures of (a) 5 MPa and (b) 300 MPa, are represented.

5. Conclusion

The present work proposes a micromechanical investigation toward the effect of grain interlocking on the behavior of rock based on simulations using the Discrete Element Method. It is shown that the degree of interlocking in the model is a function of the density of bonds linking the discrete elements.

Based on this description, the brittleness of the medium appears to be strongly related to the degree of interlocking between their constitutive particles. By implicitly modifying the microstructural properties of the medium in accordance with the texture of the rock, it is possible to accurately model some of the fundamentals aspects of brittle rock behavior such as high ratios of tensile to compressive strength (σ_c/σ_t) as well as non-linear failure envelopes. Moreover, contrary to classical DEM approaches, microparameters are relatively well correlated to the material response. For instance, local friction is directly related to the macroscopic internal friction and local cohesion is proportional to the macroscopic cohesion.

Using the proposed DEM, good agreement is achieved between laboratory test results and discrete simulations both in terms of macroscopic behavior and fracturing processes, providing a suitable approach for modeling a wide range of brittle materials, from weak to hard rocks. In addition, the model is able to reproduce a fundamental aspect of brittle failure: the formation of cracks, by degrading the cohesive strength of the medium, produces an increasing mobilization of its frictional strength with damage as described by the non-linear–linear nature of the yield envelope. The cohesive strength component controlling opening cracks dominates at low strains and at low confinement, whereas the frictional strength component dominates at large strains and high confinement. Hence, it is argued that the brittle ductile transition can be a direct result of the frictional strengthening occurring with the increase of the confinement.

Despite this relative success, additional developments are still needed to improve the theoretical basis of this numerical approach. A key point of the model is that the stored volumetric fracture energy is kept constant whatever the discretization size is (Shiu, 2009). However, in presence of large pre-existing fractures, it has been shown that the fracture toughness depends on the size of the discrete elements (Potyondy and Cundall, 2004). This comes from the fact that in the current DEM formulation, the resulting fracture thickness depends on the discretization size (Harthong et al., 2012). An improvement might be to formulate a non-local form of the fracture criterion or to consider discontinuities as volumes rather than surfaces only: this is still an open issue.

Acknowledgments

The work described in this paper was performed as part of the LOP Project's research into how failures may develop and propagate through jointed rock masses. The LOP Project is an international research and technology transfer project on the stability of rock slopes in open pit mines, established with the objective of addressing a perceived industry wide need for improved knowledge of the mechanisms of rock slope failure in open pit mines. The project is funded by a consortia of international mining companies that currently includes: Anglo American plc; AngloGold Ashanti; Barrick; BHPBilliton; Compañía Minera Dona Inès de Collahuasi SCM; De Beers; Newcrest; Newmont; Ok Tedi Mining Limited; RioTinto; Teck Resources Ltd; Vale; and Xstrata Copper.

The permission of the sponsors to present this paper is gratefully acknowledged.

References

Altindag, B., Guney, A., 2010. Predicting the relationships between brittleness and mechanical properties (UCS, TS and SH) of rocks. Sci. Res. Essays 5 (16), 2107–2118.

Brady, B.H.G., Brown, E.T., 2004. Rock mechanics for underground mining, 3rd edn. Kluwer, Dordrecht.

Brace, W.F., Paulding, B.W., Scholz, C., 1966. Dilatancy in the fracture of crystalline rocks. J. Geophys. Res. 71 (16), 3939–3953.

Byerlee, J.D., 1968. Brittle-ductile transition in rocks. J.Geophys. Res. 73 (14), 4741–4750.

Cho, N., Martin, C.D., Sego, D.C., 2007. A clumped particle model for rock. Int. J. Rock Mech. Mining Sci. 44 (7), 997–1010.

Coviello, A., Lagioia, R., Nova, R., 2005. On the measurement of the tensile strength of soft rocks. Rock Mech. Rock Eng. 38 (4), 251–273.

Donzé, F.V., Bouchez, J., Magnier, S.A., 1997. Modeling fractures in rock blasting. Int. J. Rock Mech. Mining Sci. 34 (8), 1153–1163.

Eberhardt, E., Stead, D., Stimpson, B., Read, R.S., 1998. Identifying crack initiation and propagation thresholds in brittle rock. Can. Geotech. J. 35 (2), 222–233.

Fakhimi, A., 2004. Application of slightly overlapped circular particles assembly in numerical simulation of rocks with high friction angles. Eng. Geol. 74, 129–138.

Gabet, T., Malecot, Y., Daudeville, L., 2008. Triaxial behaviour of concrete under high stresses: influence of the loading path on compaction and limit states. Cem. Concr. Res. 38 (3), 403–412.

Hajiabdolmajid, V., Kaiser, P.K., Martin, C.D., 2002. Modeling brittle failure of rock. Int. J. Rock Mech. Mining Sci. 39, 731–741.

Hart, R., Cundall, P.A., Lemos, J., 1988. Formulation of three-dimensional distinct element model Part II—mechanical calculations of a system composed of many polyhedral blocks. Int. J. Rock Mech. Mining Sci. Geomech. Abs. 25, 3117–3125.

Harthong, B., Scholtès, L., Donzé, F.V., 2012. Strength characterization of rock masses, using a coupled DEM-DFN model. Geophys. J. Int. http://dx.doi.org/10.1111/j.1365-246X.2012.05642.x.

Itasca Consulting Group Inc. 2012. PFC2D/3D (Particle Flow Code in 2/3 Dimensions), Version 4.0, Minneapolis.

Iwashita, K., Oda, M., 1998. Rolling resistance at contacts in simulation of shear band development by DEM. J. Eng. Mech. 124, 285–292.

Kazerani, T., Zhao, J., 2010. Micromechanical parameters in bonded particle method for modeling of brittle material failure. Int. J. Numer. Anal. Meth. Geomech. 34, 1877–1895.

Kozicki, J., Donzé, F.V., 2008. A new open-source software developed for numerical simulations using discrete modeling methods. Comput. Method Appl. Mech. Eng. 197 (49–50), 4429–4443.

Kozicki, J., Donzé, F.V., 2009. YADE-OPEN DEM: an open-source software using a discrete element method to simulate granular material. Eng. Comput. 26 (7), 786–805.

Lan, H., Martin, C.D., Hu, B., 2010. Effect of heterogenity of brittle rock on micromechanical extensile behavior during compression loading. J. Geophys. Res., 115, http://dx.doi.org/10.1029/2009JB006496.

Latjai, E.Z., 1969. Mechanics of second order faults and tension gashes. Geol. Soc. Am. Bull. 80, 2253–2272.

Martin, C.D., 1997. The effect of cohesion loss and stress path on brittle rock strength. Can. Geotech. J. 34, 698–725.

Martin, C.D., Chandler, N.A., 1994. The progressive failure of Lac du Bonnet granite. Int. J. Rock Mech. Mining Sci. Geomech. Abs. 31, 643–659.

Marketos, G., Bolton, M.D., 2009. Compaction bands simulated in discrete element models. J. Struct. Geol. 31 (5), 479–490.

Peng, S., Johnson, A.M., 1972. Crack growth and faulting in cylindrical specimens of Chelmsford granite. Int. J. Rock Mech. Mining Sci. 9, 37–86.

Pestman, B.J., Van Munster, J.G., 1996. An acoustic emission study of damage development and stress-memory effects in sandstone. Int. J. Rock Mech. Mining Sci. 33, 585–593.

Plassiard, J.P., Belheine, N., Donzé, F.V., 2009. A spherical discrete element model: calibration procedure and incremental response. Granul. Matter 11 (5), 293–306.

Potyondy, D.O., Cundall, P.A., 2004. A bonded-particle model for rock. Int. J. Rock Mech. Mining Sci. 41, 1329–1364.

Shiu, W., Donzé, F.V., Daudeville, L., 2008. Compaction process in concrete during missile impact: a DEM analysis. Comput. Concr. 5 (4), 329–342.

Shiu, W., 2009. Impact de missiles rigides sur structures en béton armé: analyse par la méthode des éléments discrets, PhD Thesis, Université Joseph Fourier.

Schmertmann, J.H., Osterberg, J.H., 1960. An Experimental Study of the Development of Cohesion and Friction With Axial Strain in Saturated Cohesive Soils. Research Conference on Shear Strength of Cohesive Soils. Boulder, CO, New York, American Society of Civil Engineers, 643–694.

Schofield, A.N., Worth, C.P., 1966. Critical state soil mechanics. McGraw-Hill, Maidenhead.

Scholtès, L., Donzé, F.V., Khanal, M., 2011. Scale effects on strength of geomaterials, case study: coal. J. Mech. Phys. Solids 59 (5), 1131–1146.

Scholtès, L., Donzé, F.V., 2012. Modelling progressive failure in fractured rock masses using a 3D discrete element method. Int. J. Rock Mech. Mining Sci. 52, 18–30.

Schöpfer, M., Abe, P.J., Childs, C., Walsh, J.J., 2009. The impact of porosity and crack density on the elasticity, strength and friction of cohesive granular materials: insights from DEM modeling. Int. J. Rock Mech. Mining Sci. 46 (2), 250–261.

Šmilauer, V., Catalano, E., Chareyre, B., Dorofenko S., Duriez, J., Gladky, A., Kozicki, J., Modenese, C., Scholtès, L., Sibille, L., Stránsky, J., Thoeni, K., 2010. Yade Reference Documentation. In:Smilauer, V. (Ed.), Yade Documentation, 474 1st Edition. The Yade Project, 〈http://yade-dem.org/doc/〉.

Stanchits, S., Dresen, G., 2003. Separation of tensile and shear cracks based on acoustic emission analysis of rock fracture. In: Non-Destructive Testing in Civil Engineering (NDT-CE), International Symposium, Berlin, p. 107.

Sulem, J., Ouffroukh, H., 2006. Shear banding in drained and undrained triaxial tests on a saturated sandstone: porosity and permeability evolution. Int. J. Rock Mech. Mining Sci. 43, 292–310.

Tapponier, P., Brace, W.F., 1976. Development of stress induced microcracks in Westerley granite. Int. J. Rock Mech. Mining Sci. Geomech. Abs. 13, 103–112.

Tran, V.T., Donze, F.V., Marin, P., 2011. A discrete element model of concrete under high triaxial loading. Cem. Concr. Compos. 33 (9), 936–948.

Wang, Y., Tonon, F., 2009. Modeling Lac du Bonnet granite using a discrete element model. Int. J. Rock Mech. Mining Sci. 46, 1124–1135.

Wang, Y., Mora, P., 2008, Modeling Wing Crack Extension: Im-plications for the Ingredients of Discrete Element Model, 165, 609–620.